THE JOURNAL OF PHYSICAL CHEMISTRY C

Article

Cite This: J. Phys. Chem. C 2018, 122, 23978−23984

pubs.acs.org/JPCC

Composition Screening of Lithium- and Sodium-Rich Anti-Perovskites for Fast-Conducting Solid Electrolytes

James A. Dawson,* Hungru Chen, and M. Saiful Islam*

Department of Chemistry, University of Bath, Bath, BA2 7AY, United Kingdom

Supporting Information

ABSTRACT: Li- and Na-rich anti-perovskites are receiving increasing attention as high-performance solid electrolytes for applications within all-solid-state batteries. The defect chemistry and ionic transport in a wide range of $Li_{3-x}Na_xOCl_{1-y}Br_y$ compositions are examined using advanced materials modeling techniques. Our calculations indicate that alkali-halide Schottky defect pairs are the dominant type of intrinsic disorder in these materials. Li-ion conductivity is shown to significantly exceed Na-ion conductivity, with the highest conductivities found for Li_3OCl and Li_3OBr. The effect of Cl/Br mixing on conductivity is shown to be small but could be used to fine-tune the activation energy. Both low conductivities and high activation energy barriers are found for the mixed Li/Na systems, which suggests that they would make poor solid electrolytes. The results presented here will aid the future optimization of anti-perovskite materials for solid electrolyte applications.

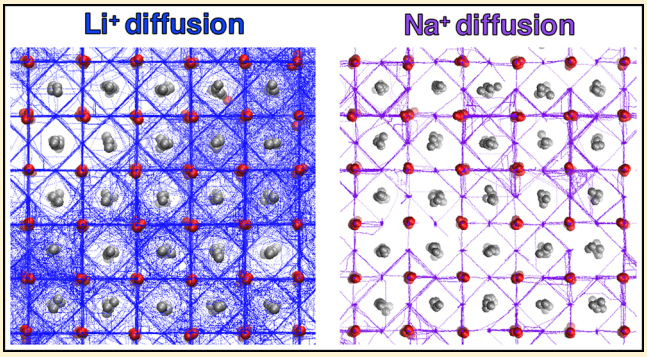

INTRODUCTION

Solid-state Li- and Na-ion batteries are currently attracting considerable interest, as they possess a number of potential advantages compared to liquid electrolyte systems, including energy density gains, improved safety, and reduced costs.[1−8] As a result, research into new solid electrolyte materials with high ionic conductivity, stability, and electrode compatibility has increased dramatically in recent years. However, numerous unresolved challenges still remain for the development of all-solid-state batteries, including low ionic conductivity and interfacial issues.[5,9−14]

Li-rich anti-perovskites (Li_3OX, where X = Cl or Br) represent a new family of solid electrolyte materials, inspired by the high-temperature superionic conductivity of $NaMgF_3$ and $(K,Na)MgF_3$ perovskites.[15] These materials possess a number of advantages in solid electrolyte applications, such as high ionic conductivity with low migration barriers for Li- and Na-ion transport, negligible electronic conductivity, wide electrochemical windows, stable operation, good cyclability, and cheap, environmentally friendly raw materials.[15−27] Another important advantage of the ubiquitous perovskite structure is the ease in which it can be modified chemically and structurally in order to optimize ionic conductivity.[15,28−32] Shortly after the reports of high Li-ion conductivity in Li_3OX (X = Cl or Br), Na analogues were investigated, with several studies analyzing the ionic conductivity and stability of Na_3OX (X = Cl or Br).[33−35] As an alternative to Li-ion batteries, Na-ion batteries have the notable advantage of raw material abundance (and therefore reduced cost) and are mostly used for large-scale grid applications.[36−38]

An early study of Li_3OCl, Li_3OBr, and $Li_3OCl_{0.5}Br_{0.5}$ as solid electrolytes noted their high ionic conductivities of $>10^{-3}$ S cm^{-1} at room temperature and low activation energies of 0.2−0.3 eV.[15] However, since this study, there have been numerous reports of significantly higher activation energies (~0.6 eV) and lower conductivities (10^{-6} S cm^{-1} at room temperature) for bulk Li_3OCl and Li_3OBr,[16,25−27] with high grain boundary resistance being proposed as an explanation for such differences.[16,25,27,39] Computational studies have also been conducted to help understand some of the interesting behavior of these potential electrolyte materials, including ion migration mechanisms, defect chemistry, and stability.[18,19,24,33−35,39−49]

Despite the recent interest in these anti-perovskites, there are still a number of unanswered questions regarding their conductivity mechanisms and the effect of halide (Cl/Br) and cation (Li/Na) mixing, especially for the Na-based materials. Therefore, there is a direct need for a systematic study of their defect formation and composition optimization, as they have not been fully characterized.

Here, we use potential-based energy minimization and molecular dynamics (MD) calculations to investigate defect formation and Li- and Na-ion transport in solid solutions of $Li_{3-x}Na_xOCl_{1-y}Br_y$ anti-perovskites. We first consider the formation of intrinsic defects in order to identify which defects are dominant in these systems and how this influences the conduction mechanisms. The ion conductivity properties of

Received: August 23, 2018
Revised: September 26, 2018
Published: September 26, 2018

DOI: 10.1021/acs.jpcc.8b08208
J. Phys. Chem. C 2018, 122, 23978−23984

the compositions are then computed using large-scale MD calculations for a range of temperatures and vacancy concentrations. To the best of our knowledge, this is the only study to directly compare Li- and Na-based anti-perovskite solid electrolytes. The results presented here help to provide a framework that can be used to guide future experimental syntheses of these anti-perovskite materials in an attempt to optimize their ionic conductivity.

METHODOLOGY

The calculations are based on well-established techniques and have been widely used to investigate the defect and ion transport properties of a wide range of ionic solids.[50,51] The short-range forces are accounted for by interatomic potentials (Buckingham type) and the long-range ionic interactions treated using Coulombic terms. Formal valence charges were used for all ions, with ionic polarization taken into account by the shell model.[52] The Mott−Littleton approximation,[53] as implemented in the GULP code,[54] was used for all defect calculations.

The potential model of Mouta et al.[42] was used for all anti-perovskite systems considered, with a number of refinements[55−59] to find the best agreement in terms of lattice parameters, bond lengths, and bulk moduli. Information regarding the development of the potential model is available in the Supporting Information, and the utilized potential parameters are listed in Table S1.

The LAMMPS code[60] was used for all MD calculations. Long MD runs of 10 ns were completed using a time step of 2 fs with supercells of ∼5000 ions. Simulations were carried out for a temperature range of 500−1000 K at intervals of 100 K using the NPT ensemble with a Nosé−Hoover thermostat.[61] Conductivities were obtained from self-diffusion data from mean-squared displacements (MSDs) using the Nernst−Einstein relation, with a Haven ratio of 1. To counter the variability that can sometimes occur with MSDs,[62] three test runs were carried out for Li_3OCl at various temperatures, with no major change to the main findings in this study. It should be noted that the large supercells, numerous configurations, and long time scales employed in this study would not be possible using ab initio MD. An example LAMMPS input file used is available in the Supporting Information. Both the defect and MD calculations used in this work have been successfully applied to a wide range of Li- and Na-ion battery materials.[39,45,63−69]

RESULTS AND DISCUSSION

Structures and Intrinsic Defect Chemistry. In the conventional perovskite structure, ABX_3, the A and B sites are cations and the X site is an anion, as in $CaTiO_3$. In the anti-perovskite structure, the A and B sites are occupied by anions (halide and oxide, respectively, in our structure) and the X site is a cation (Li or Na in our structure). In $Li_{3-x}Na_xOCl_{1-y}Br_y$, the central B-site oxygen ion is octahedrally coordinated to six Li or Na ions. The corner A-site halogens are cuboctahedrally coordinated to 12 nearest-neighbor Li or Na ions.

We first computed the structures of the end-member anti-perovskites, i.e., Li_3OCl, Li_3OBr, Na_3OCl, and Na_3OBr. A comparison of the calculated and experimental lattice parameters is given in Table 1; the differences between them are minute (<0.5%), meaning that the derived potential model can adequately reproduce the experimental structures of these materials.

Table 1. Comparison of Calculated and Experimental Lattice Parameters (Å) for Li_3OCl, Li_3OBr, Na_3OCl, and Na_3OBr

system	a (calculated)	a (experimental)	diff. %
Li_3OCl	3.921	3.907[70]	0.36
Li_3OBr	4.024	4.035[26]	0.27
Na_3OCl	4.501	4.496[71]	0.11
Na_3OBr	4.579	4.567[34]	0.26

In addition, we also considered a number of mixed systems, namely, $Li_3OCl_{0.5}Br_{0.5}$, $Na_3OCl_{0.5}Br_{0.5}$, Li_2NaOCl, Li_2NaOBr, $LiNa_2OCl$, and $LiNa_2OBr$. A number of halide configurations were tested for these mixed halide structures. As the variation in the lattice energies of the tested configurations was small (<0.1 eV), we used a structure with an alternating arrangement of Cl and Br ions for the defect and MD calculations. For the mixed cation systems, layered structures with alternating layers of Li and Na in the ab plane were used, as they were energetically more favorable than random arrangements. The calculated lattice parameters for the mixed configurations are provided in Table S2. As expected, the lattice parameters for $Li_3OCl_{0.5}Br_{0.5}$ (3.973 Å) and $Na_3OCl_{0.5}Br_{0.5}$ (4.537 Å) are averages of those for their respective end members. For the mixed cation configurations, tetragonal unit cells were formed as a result of the deformed OLi_4Na_2 and OLi_2Na_4 polyhedra, which are a consequence of the size difference between Li and Na ions.

To gain insight into the defect chemistry of these materials, we computed the energetics of intrinsic Frenkel- and Schottky-type defects in the anti-perovskite end members and mixed configurations. As examples, the main defects that we focus on for Li_3OCl are given below in Kröger−Vink notation:

Li Frenkel:

$$Li_{Li}^{x} \rightarrow V_{Li}^{/} + Li_i^{\bullet} \quad (1)$$

Full Schottky:

$$3Li_{Li}^{x} + O_O^{x} + Cl_{Cl}^{x} \rightarrow 3V_{Li}^{/} + V_O^{\bullet\bullet} + V_{Cl}^{\bullet} + Li_3OCl \quad (2)$$

LiCl Partial Schottky:

$$Li_{Li}^{x} + Cl_{Cl}^{x} \rightarrow V_{Li}^{/} + V_{Cl}^{\bullet} + LiCl \quad (3)$$

Equivalent equations for the Na- and Br-based systems can be formulated by simply replacing the relevant ions. The formation energies for these intrinsic defects in the end-member and mixed systems are displayed in Figure 1. The cation Frenkel and alkali-halide partial Schottky defects represent the most favorable types of intrinsic disorder in these materials.

Several key points can be made on the basis of the results in Figure 1. First, the energies for intrinsic disorder in these materials are generally high, suggesting that the defect concentrations will be low. Second, the alkali-halide Schottky pair (eq 3) is the lowest energy defect in the majority of cases. This agrees with previous findings for Li_3OCl,[24] which also state that it is responsible for the creation of low energy Li pathways for Li_3OCl. The higher energies for cation Frenkel pairs indicate that the concentration of metal interstitials in these materials is low, as also found by density functional

DOI: 10.1021/acs.jpcc.8b08208
J. Phys. Chem. C 2018, 122, 23978−23984

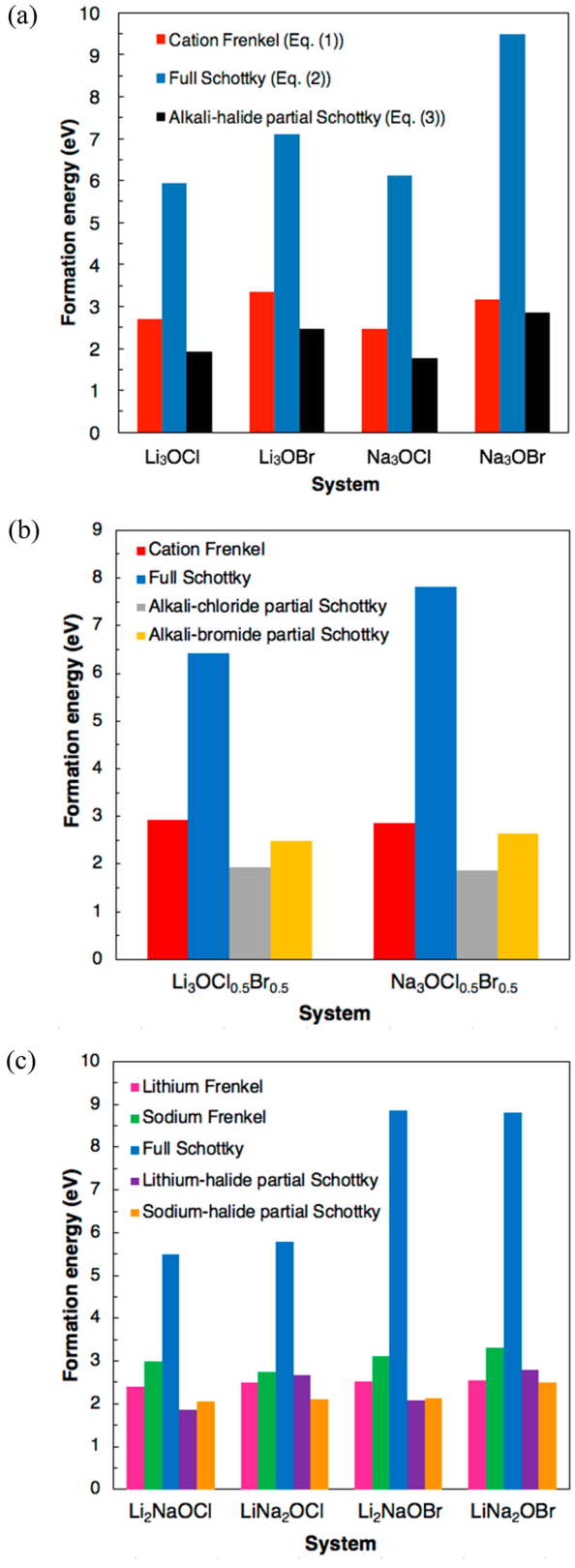

Figure 1. Formation energies of intrinsic defects (eV) for the (a) end-member compositions Li_3OX and Na_3OX (X = Cl or Br), the (b) mixed halide systems $Li_3OCl_{0.5}Br_{0.5}$ and $Na_3OCl_{0.5}Br_{0.5}$, and the (c) mixed cation systems Li_2NaOCl, $LiNa_2OCl$, Li_2NaOBr, and $LiNa_2OBr$.

theory calculations of Li_3OCl and Li_3OBr.[40] Interestingly, in the mixed cation systems, the most favorable partial Schottky includes the cation that is in the majority, e.g., Na in $LiNa_2OBr$. Our calculated values are in good agreement with previous potentials-based and density functional theory calculations for Li_3OCl.[24,42]

These results suggest that Li and Na vacancy hopping is the main transport mechanism in these anti-perovskites, as opposed to interstitial diffusion. Finally, the results suggest that intrinsic disorder in the Br-based systems is less favorable than that for the Cl-based systems, which is likely to have a significant effect on their electrochemical performance.

Li- and Na-Ion Conduction and Dynamics. We use long time scale MD calculations of $Li_{3-x}Na_xOCl_{1-y}Br_y$ compositions with representative concentrations of alkali-halide partial Schottky defects; for example, $Li_{3-\delta}OCl_{1-\delta}$, where δ = 0.038 or 0.150, to examine the Li- and Na-ion conductivity. The MD calculations were run over a long simulation time of 10 ns and for a large temperature range of 500−1000 K.

The plots of MSDs for the end-member and mixed systems at a representative temperature of 700 K and an alkali-halide partial Schottky defect concentration of δ = 0.038 are given in Figures S1 and S2, respectively. We can derive the Li and Na diffusion coefficients using the MSD data and then convert them to ionic conductivities using the Nernst−Einstein equation.

Figure 2a shows representative Arrhenius plots for Li- and Na-ion conductivity for Li_3OX and Na_3OX (X = Cl or Br) with an alkali-halide partial Schottky defect concentration of δ = 0.038. As expected, the Li-based systems exhibit the highest conductivities of ~5×10^{-3} S cm^{-1} at 500 K. These values are in good agreement with the experimental reports in the literature[16] and in excellent agreement with the only previous potentials-based MD study, which only considered Li_3OCl.[24] The conductivities of Na_3OCl and Na_3OBr are over 1 order of magnitude lower than the Li-based materials, with values of ~2×10^{-4} S cm^{-1} at 500 K. Again, these values are in excellent agreement with experiment.[33] However, it should be noted that Wang et al.[33] predicted the conductivity of Na_3OBr to be higher than that of Na_3OCl, albeit with a higher activation energy. The conductivity of the Cl-based materials is marginally higher than that for the equivalent Br-based materials.

The conductivities for the mixed systems are plotted in Figure 2b. For the mixed halide systems, the conductivities of 3.56×10^{-3} and 1.26×10^{-4} S cm^{-1} at 500 K for $Li_3OCl_{0.5}Br_{0.5}$ and $Na_3OCl_{0.5}Br_{0.5}$, respectively, are slightly lower than those for the respective end-member materials. The Li-ion conductivities of the Li_2NaOCl and Li_2NaOBr systems (3.99×10^{-4} and 6.32×10^{-4} S cm^{-1}, respectively, at 500 K) are around 1 order of magnitude lower than those for Li_3OCl and Li_3OBr. The equivalent values for $LiNa_2OCl$ and $LiNa_2OBr$ (1.66 and 1.18 S cm^{-1}, respectively, at 500 K) are similar to those for Na_3OCl and Na_3OBr. Li-ion conductivity is notably higher than Na-ion conductivity in these materials. On the basis of conductivity alone, the mixed systems do not exhibit any substantial improved performance compared to Li_3OX and Na_3OX (X = Cl or Br).

We also analyzed the effect of alkali-halide partial Schottky defect concentration on conductivity, as shown in Figure S3 for Li_3OCl. It is clear that conductivity increases with increasing Li/Cl vacancy concentration. This is not surprising given that a vacancy mechanism is reported for these materials, both in the literature and from our own results. Previous calculations have shown that the binding between Li and Cl

DOI: 10.1021/acs.jpcc.8b08208
J. Phys. Chem. C 2018, 122, 23978−23984

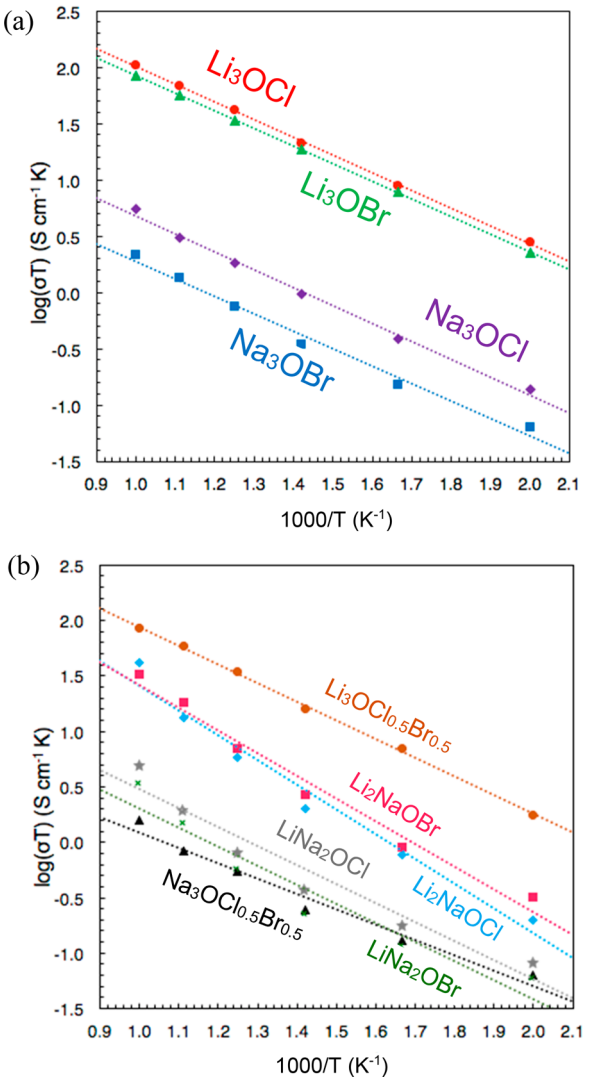

Figure 2. Arrhenius plots of temperature-dependent Li^+ and Na^+ ionic conductivity for the (a) end members and (b) mixed systems with an alkali-halide partial Schottky defect concentration of δ = 0.038. Conductivities are plotted for the majority cations in the mixed cation systems.

vacancies is notably low compared to other defect pairs in Li_3OCl.[24] The increase in Li conductivity can be as high as 60% when moving from δ = 0.038 to 0.150. The results presented here are representative of the other simulated systems and are in agreement with previous calculations.[24]

The calculated activation energies for Li- and Na-ion conductivity in each system are given in Table 2. The activation energies for Li_3OX and Na_3OX, X = Cl or Br, are similar, with values ranging from 0.26 to 0.31 eV. Comparison to experiment shows significant underestimations for our calculated values, which strongly indicates the presence of highly resistive grain boundaries and/or interfacial effects in the experimental samples.[39] Our values do, however, agree well with previous MD and NEB calculations.[24,33,34,41] The activation energies for Na_3OCl and Na_3OBr are marginally lower than those for Li_3OCl and Li_3OBr. This finding agrees with the similarity in activation energies for these systems obtained by NEB calculations.[24,33,34,41] The effect of vacancy concentration on the activation energies of these systems is relatively weak, with marginal decreases in activation energy observed with increasing vacancy concentration.

Table 2. Activation Energies (eV) of Li- and Na-Ion Conductivity in the (a) End Member, Mixed Halide and (b) Mixed Cation Systems for Alkali-Halide Partial Schottky Defect Concentrations of δ = 0.038 and 0.150

(a)

system	δ = 0.038	δ = 0.150
Li_3OCl	0.29	0.27
Li_3OBr	0.31	0.29
Na_3OCl	0.29	0.26
Na_3OBr	0.28	0.26
$Li_3OCl_{0.5}Br_{0.5}$	0.31	0.32
$Na_3OCl_{0.5}Br_{0.5}$	0.24	0.22

(b)

	δ = 0.038		δ = 0.150	
system	Li	Na	Li	Na
Li_2NaOCl	0.41	0.40	0.61	0.67
Li_2NaOBr	0.38	0.44	0.58	0.67
$LiNa_2OCl$	0.25	0.31	0.44	0.43
$LiNa_2OBr$	0.30	0.31	0.42	0.44

For the mixed halide systems, there is a notable difference between the two sets of activation energies. For $Li_3OCl_{0.5}Br_{0.5}$, the values are very similar to Li_3OCl and Li_3OBr; however, for $Na_3OCl_{0.5}Br_{0.5}$, the energies are lower than those for both Na_3OCl and Na_3OBr, and are the lowest calculated for any of the simulated systems. Although these low activation energies suggest that $Na_3OCl_{0.5}Br_{0.5}$ could be an interesting candidate for solid electrolytes, both experiment[26] and our calculations have shown that the conductivity of this system does not exceed that of the Na_3OCl and Na_3OBr end members. This illustrates that, although halide mixing may not produce a dramatic increase in conductivity, it can perhaps be used to tune the activation energy.

In comparison to the other systems, the activation energies for the mixed cation systems are generally high, particularly for Li_2NaOCl and Li_2NaOBr. We can see that the vast majority of Na-ion activation energies are higher than the equivalent Li-ion activation energies in these mixed cation structures. Given these results and the limited ionic diffusion and conductivity shown in Figure 2b, respectively, it is unlikely that these materials can be used for high-performance solid electrolytes.

The trends illustrated by the conductivities and activation energies can also be directly visualized by analyzing the Li-ion trajectories accumulated during the 10 ns MD simulations. Figure 3 shows the Li- and Na-ion diffusion density maps for Li_3OCl, Na_3OCl, and Li_2NaOCl with an alkali-halide partial Schottky defect concentration of δ = 0.038 at 700 K. First, it can be seen that the largest Li- and Na-ion densities are located around the crystallographic sites, as expected, with significant amounts of local oscillation. Second, we can also see that some Li and Na ions diffuse to adjacent sites both diagonally and laterally as a result of the vacant sites, thereby creating long-range diffusion pathways. Third, the differences in conductivity between these three systems can be visualized, with the density map of the system with the highest ion conduction, Li_3OCl (Figure 3a), showing the strongest long-range ion transport.

DOI: 10.1021/acs.jpcc.8b08208
J. Phys. Chem. C 2018, 122, 23978−23984

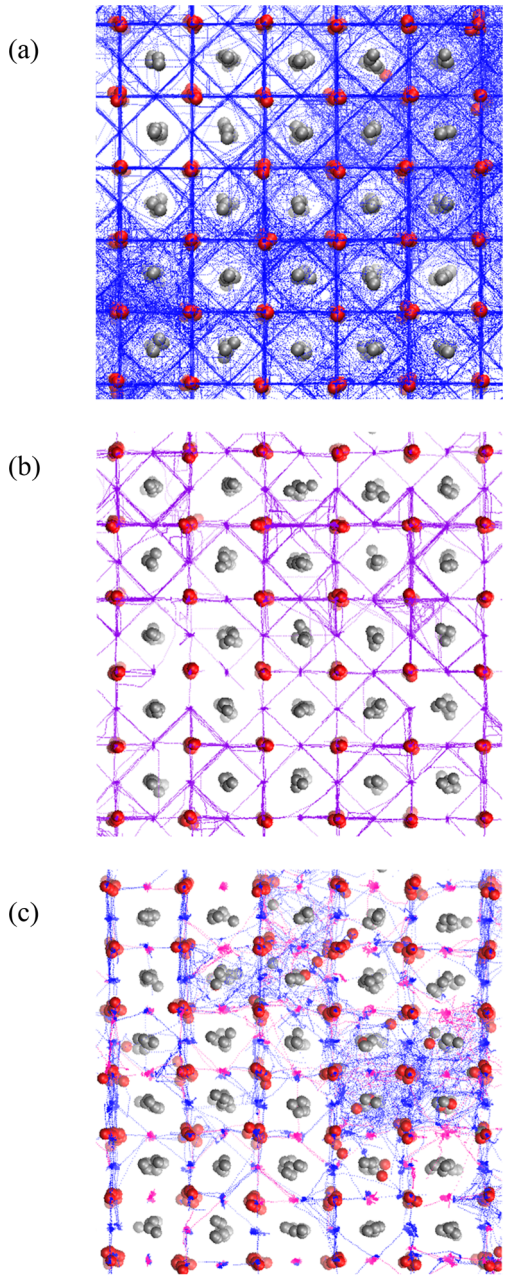

Figure 3. Trajectory plots of (a) Li ions (blue) in Li_3OCl, (b) Na ions (purple) in Na_3OCl, and (c) Li and Na ions in Li_2NaOCl with an alkali-chloride partial Schottky defect concentration of δ = 0.038 at 700 K for 10 ns simulations. O and Cl ions are given in red and silver, respectively.

CONCLUSIONS

We have investigated the defect chemistry and ion transport of a wide range of anti-perovskite compositions based on Li_3OCl and Na_3OCl (X = Cl, Br) for their potential use as solid electrolytes in Li- and Na-ion batteries. We have confirmed that Schottky vacancy defects are the dominant type of intrinsic disorder in these materials. The highest conductivities of ~5 × 10^{-3} S cm^{-1} (500 K) are obtained for Li_3OCl and Li_3OBr. The effect of halide-ion mixing on conductivity is shown to be small but could be used to fine-tune the activation energy. Low conductivities and high activation energy barriers are predicted for the mixed Li/Na systems, which are likely to inhibit their performance as solid-state electrolytes.

This is the first study to consider such a large number of anti-perovskite systems as solid electrolyte materials, and the results will help guide their future optimization for energy storage applications.

ASSOCIATED CONTENT

Supporting Information

The Supporting Information is available free of charge on the ACS Publications website at DOI: 10.1021/acs.jpcc.8b08208.

Tables S1 and S2 listing potential parameters used and lattice parameters of mixed systems; Figures S1−S3 showing mean-squared displacement plots for all systems at 700 K and Arrhenius plots of temperature-dependent Li^+ ionic conductivity for Li_3OCl with a range of alkali-halide partial Schottky defect concentrations; example LAMMPS input file (PDF)

AUTHOR INFORMATION

Corresponding Authors

*E-mail: j.a.dawson@bath.ac.uk.
*E-mail: m.s.islam@bath.ac.uk.

ORCID

James A. Dawson: 0000-0002-3946-5337
M. Saiful Islam: 0000-0003-3882-0285

Notes

The authors declare no competing financial interest.

ACKNOWLEDGMENTS

The authors gratefully acknowledge the EPSRC Programme Grant "Enabling next generation lithium batteries" (EP/M009521/1) and the MCC/Archer consortium (EP/L000202/1).

REFERENCES

(1) Manthiram, A.; Yu, X.; Wang, S. Lithium Battery Chemistries Enabled by Solid-State Electrolytes. *Nat. Rev. Mater.* **2017**, *2*, 16103.
(2) Janek, J.; Zeier, W. G. A Solid Future for Battery Development. *Nat. Energy* **2016**, *1*, 16141.
(3) Tikekar, M. D.; Choudhury, S.; Tu, Z.; Archer, L. A. Design Principles for Electrolytes and Interfaces for Stable Lithium-Metal Batteries. *Nat. Energy* **2016**, *1*, 16114.
(4) Bachman, J. C.; Muy, S.; Grimaud, A.; Chang, H.-H.; Pour, N.; Lux, S. F.; Paschos, O.; Maglia, F.; Lupart, S.; Lamp, P.; et al. Inorganic Solid-State Electrolytes for Lithium Batteries: Mechanisms and Properties Governing Ion Conduction. *Chem. Rev.* **2016**, *116*, 140−162.
(5) Kerman, K.; Luntz, A.; Viswanathan, V.; Chiang, Y.-M.; Chen, Z. Review—Practical Challenges Hindering the Development of Solid State Li Ion Batteries. *J. Electrochem. Soc.* **2017**, *164*, A1731−A1744.
(6) Zhou, W.; Li, Y.; Xin, S.; Goodenough, J. B. Rechargeable Sodium All-Solid-State Battery. *ACS Cent. Sci.* **2017**, *3*, 52−57.
(7) Kim, J.-J.; Yoon, K.; Park, I.; Kang, K. Progress in the Development of Sodium-Ion Solid Electrolytes. *Small Methods* **2017**, *1*, 1700219.
(8) Richards, W. D.; Tsujimura, T.; Miara, L. J.; Wang, Y.; Kim, J. C.; Ong, S. P.; Uechi, I.; Suzuki, N.; Ceder, G. Design and Synthesis of the Superionic Conductor $Na_{10}SnP_2S_{12}$. *Nat. Commun.* **2016**, *7*, 11009.
(9) Luntz, A. C.; Voss, J.; Reuter, K. Interfacial Challenges in Solid-State Li Ion Batteries. *J. Phys. Chem. Lett.* **2015**, *6*, 4599−4604.
(10) Yu, C.; Ganapathy, S.; van Eck, E. R. H.; Wang, H.; Basak, S.; Li, Z.; Wagemaker, M. Accessing the Bottleneck in All-Solid State Batteries, Lithium-Ion Transport over the Solid-Electrolyte-Electrode Interface. *Nat. Commun.* **2017**, *8*, 1086.

DOI: 10.1021/acs.jpcc.8b08208
J. Phys. Chem. C 2018, 122, 23978−23984

(11) Lotsch, B. V.; Maier, J. Relevance of Solid Electrolytes for Lithium-Based Batteries: A Realistic View. *J. Electroceram.* **2017**, *38*, 128−141.
(12) Richards, W. D.; Miara, L. J.; Wang, Y.; Kim, J. C.; Ceder, G. Interface Stability in Solid-State Batteries. *Chem. Mater.* **2016**, *28*, 266−273.
(13) Ma, C.; Chi, M. Novel Solid Electrolytes for Li-Ion Batteries: A Perspective from Electron Microscopy Studies. *Front. Energy Res.* **2016**, *4*, 23.
(14) Canepa, P.; Dawson, J. A.; Sai Gautam, G.; Statham, J. M.; Parker, S. C.; Islam, M. S. Particle Morphology and Lithium Segregation to Surfaces of the $Li_7La_3Zr_2O_{12}$ Solid Electrolyte. *Chem. Mater.* **2018**, *30*, 3019−3027.
(15) Zhao, Y.; Daemen, L. L. Superionic Conductivity in Lithium-Rich Anti-Perovskites. *J. Am. Chem. Soc.* **2012**, *134*, 15042−15047.
(16) Lü, X.; Howard, J. W.; Chen, A.; Zhu, J.; Li, S.; Wu, G.; Dowden, P.; Xu, H.; Zhao, Y.; Jia, Q. Antiperovskite Li_3OCl Superionic Conductor Films for Solid-State Li-Ion Batteries. *Adv. Sci.* **2016**, *3*, 1500359.
(17) Braga, M. H.; Ferreira, J. a.; Stockhausen, V.; Oliveira, J. E.; El-Azab, A. Novel Li_3ClO Based Glasses with Superionic Properties for Lithium Batteries. *J. Mater. Chem. A* **2014**, *2*, 5470.
(18) Fang, H.; Wang, S.; Liu, J.; Sun, Q.; Jena, P. Superhalogen-Based Lithium Superionic Conductors. *J. Mater. Chem. A* **2017**, *5*, 13373−13381.
(19) Song, A.-Y.; Xiao, Y.; Turcheniuk, K.; Upadhya, P.; Ramanujapuram, A.; Benson, J.; Magasinski, A.; Olguin, M.; Meda, L.; Borodin, O. Protons Enhance Conductivities in Lithium Halide Hydroxide/Lithium Oxyhalide Solid Electrolytes by Forming Rotating Hydroxy Groups. *Adv. Energy Mater.* **2018**, *8*, 1700971.
(20) Braga, M. H.; Murchison, A. J.; Ferreira, J. A.; Singh, P.; Goodenough, J. B. Glass-Amorphous Alkali-Ion Solid Electrolytes and Their Performance in Symmetrical Cells. *Energy Environ. Sci.* **2016**, *9*, 948−954.
(21) Li, Y.; Zhou, W.; Xin, S.; Li, S.; Zhu, J.; Lü, X.; Cui, Z.; Jia, Q.; Zhou, J.; Zhao, Y.; et al. Fluorine-Doped Antiperovskite Electrolyte for All-Solid-State Lithium-Ion Batteries. *Angew. Chem., Int. Ed.* **2016**, *55*, 9965−9968.
(22) Braga, M. H.; Grundish, N. S.; Murchison, A. J.; Goodenough, J. B. Alternative Strategy for a Safe Rechargeable Battery. *Energy Environ. Sci.* **2017**, *10*, 331−336.
(23) Hood, Z. D.; Wang, H.; Samuthira Pandian, A.; Keum, J. K.; Liang, C. Li_2OHCl Crystalline Electrolyte for Stable Metallic Lithium Anodes. *J. Am. Chem. Soc.* **2016**, *138*, 1768−1771.
(24) Lu, Z.; Chen, C.; Baiyee, Z. M.; Chen, X.; Niu, C.; Ciucci, F. Defect Chemistry and Lithium Transport in Li_3OCl Anti-Perovskite Superionic Conductors. *Phys. Chem. Chem. Phys.* **2015**, *17*, 32547−32555.
(25) Lu, X.; Wu, G.; Howard, J. W.; Chen, A.; Zhao, Y.; Daemen, L. L.; Jia, Q. Li-Rich Anti-Perovskite Li_3OCl Films with Enhanced Ionic Conductivity. *Chem. Commun.* **2014**, *50*, 11520−11522.
(26) Zhu, J.; Li, S.; Zhang, Y.; Howard, J. W.; Lu, X.; Li, Y.; Wang, Y.; Kumar, R. S.; Wang, L.; Zhao, Y. Enhanced Ionic Conductivity with $Li_7O_2Br_3$ Phase in Li_3OBr Anti-Perovskite Solid Electrolyte. *Appl. Phys. Lett.* **2016**, *109*, 101904.
(27) Li, S.; Zhu, J.; Wang, Y.; Howard, J. W.; Lü, X.; Li, Y.; Kumar, R. S.; Wang, L.; Daemen, L. L.; Zhao, Y. Reaction Mechanism Studies towards Effective Fabrication of Lithium-Rich Anti-Perovskites Li_3OX (X = Cl, Br). *Solid State Ionics* **2016**, *284*, 14−19.
(28) Peña, M. A.; Fierro, J. L. G. Chemical Structures and Performance of Perovskite Oxides. *Chem. Rev.* **2001**, *101*, 1981−2018.
(29) Bonanos, N.; Knight, K. S.; Ellis, B. Perovskite Solid Electrolytes: Structure, Transport Properties and Fuel Cell Applications. *Solid State Ionics* **1995**, *79* (Suppl. C), 161−170.
(30) Bhalla, A. S.; Guo, R.; Roy, R. The Perovskite Structure − a Review of Its Role in Ceramic Science and Technology. *Mater. Res. Innovations* **2000**, *4*, 3−26.
(31) Dawson, J. A.; Naylor, A. J.; Eames, C.; Roberts, M.; Zhang, W.; Snaith, H. J.; Bruce, P. G.; Islam, M. S. Mechanisms of Lithium Intercalation and Conversion Processes in Organic−Inorganic Halide Perovskites. *ACS Energy Lett.* **2017**, *2*, 1818−1824.
(32) Dawson, J. A.; Chen, H.; Tanaka, I. Crystal Structure, Defect Chemistry and Oxygen Ion Transport of the Ferroelectric Perovskite, $Na_{0.5}Bi_{0.5}TiO_3$: Insights from First-Principles Calculations. *J. Mater. Chem. A* **2015**, *3*, 16574−16582.
(33) Wang, Y.; Wang, Q.; Liu, Z.; Zhou, Z.; Li, S.; Zhu, J.; Zou, R.; Wang, Y.; Lin, J.; Zhao, Y. Structural Manipulation Approaches towards Enhanced Sodium Ionic Conductivity in Na-Rich Anti-perovskites. *J. Power Sources* **2015**, *293*, 735−740.
(34) Zhu, J.; Wang, Y.; Li, S.; Howard, J. W.; Neuefeind, J.; Ren, Y.; Wang, H.; Liang, C.; Yang, W.; Zou, R.; et al. Sodium Ion Transport Mechanisms in Antiperovskite Electrolytes Na_3OBr and Na_4OI_2: An in Situ Neutron Diffraction Study. *Inorg. Chem.* **2016**, *55*, 5993−5998.
(35) Nguyen, H.; Hy, S.; Wu, E.; Deng, Z.; Samiee, M.; Yersak, T.; Luo, J.; Ong, S. P.; Meng, Y. S. Experimental and Computational Evaluation of a Sodium-Rich Anti-Perovskite for Solid State Electrolytes. *J. Electrochem. Soc.* **2016**, *163*, A2165−A2171.
(36) Yabuuchi, N.; Kubota, K.; Dahbi, M.; Komaba, S. Research Development on Sodium-Ion Batteries. *Chem. Rev.* **2014**, *114*, 11636−11682.
(37) Palomares, V.; Serras, P.; Villaluenga, I.; Hueso, K. B.; Carretero-González, J.; Rojo, T. Na-Ion Batteries, Recent Advances and Present Challenges to Become Low Cost Energy Storage Systems. *Energy Environ. Sci.* **2012**, *5*, 5884.
(38) Hwang, J.-Y.; Myung, S.-T.; Sun, Y.-K. Sodium-Ion Batteries: Present and Future. *Chem. Soc. Rev.* **2017**, *46*, 3529−3614.
(39) Dawson, J. A.; Canepa, P.; Famprikis, T.; Masquelier, C.; Islam, M. S. Atomic-Scale Influence of Grain Boundaries on Li-Ion Conduction in Solid Electrolytes for All-Solid-State Batteries. *J. Am. Chem. Soc.* **2018**, *140*, 362−368.
(40) Emly, A.; Kioupakis, E.; Van der Ven, A. Phase Stability and Transport Mechanisms in Antiperovskite Li_3OCl and Li_3OBr Superionic Conductors. *Chem. Mater.* **2013**, *25*, 4663−4670.
(41) Deng, Z.; Radhakrishnan, B.; Ong, S. P. Rational Composition Optimization of the Lithium-Rich $Li_3OCl_{1-X}Br_x$ Anti-Perovskite Superionic Conductors. *Chem. Mater.* **2015**, *27*, 3749−3755.
(42) Mouta, R.; Melo, M. Á. B.; Diniz, E. M.; Paschoal, C. W. A. Concentration of Charge Carriers, Migration, and Stability in Li_3OCl Solid Electrolytes. *Chem. Mater.* **2014**, *26*, 7137−7144.
(43) Howard, J.; Hood, Z. D.; Holzwarth, N. A. W. Fundamental Aspects of the Structural and Electrolyte Properties of Li_2OHCl from Simulations and Experiment. *Phys. Rev. Mater.* **2017**, *1*, 75406.
(44) Wang, Z.; Xu, H.; Xuan, M.; Shao, G. From Anti-Perovskite to Double Anti-Perovskite: Tuning Lattice Chemistry to Achieve Super-Fast Li^+ Transport in Cubic Solid Lithium Halogen-Chalcogenides. *J. Mater. Chem. A* **2018**, *6*, 73−83.
(45) Dawson, J. A.; Attari, T. S.; Chen, H.; Emge, S. P.; Johnston, K. E.; Islam, M. S. Elucidating Lithium-Ion and Proton Dynamics in Anti-Perovskite Solid Electrolytes. *Energy Environ. Sci.* **2018**, *11*, 2993.
(46) Wan, T. H.; Lu, Z.; Ciucci, F. A First Principle Study of the Phase Stability, Ion Transport and Substitution Strategy for Highly Ionic Conductive Sodium Antipervoskite as Solid Electrolyte for Sodium Ion Batteries. *J. Power Sources* **2018**, *390*, 61−70.
(47) Zhang, Y.; Zhao, Y.; Chen, C. Ab Initio Study of the Stabilities of and Mechanism of Superionic Transport in Lithium-Rich Antiperovskites. *Phys. Rev. B: Condens. Matter Mater. Phys.* **2013**, *87*, 134303.
(48) Stegmaier, S.; Voss, J.; Reuter, K.; Luntz, A. C. Li^+ Defects in a Solid-State Li Ion Battery: Theoretical Insights with a Li_3OCl Electrolyte. *Chem. Mater.* **2017**, *29*, 4330−4340.
(49) Chen, M.-H.; Emly, A.; Van der Ven, A. Anharmonicity and Phase Stability of Antiperovskite Li_3OCl. *Phys. Rev. B: Condens. Matter Mater. Phys.* **2015**, *91*, 214306.
(50) Islam, M. S.; Fisher, C. A. J. Lithium and Sodium Battery Cathode Materials: Computational Insights into Voltage, Diffusion and Nanostructural Properties. *Chem. Soc. Rev.* **2014**, *43*, 185−204.
(51) Catlow, C. R. A. *Computational Approaches to Energy Materials*; Wiley: Chichester, U.K., 2013.

DOI: 10.1021/acs.jpcc.8b08208
J. Phys. Chem. C 2018, 122, 23978−23984

(52) Dick, B. G.; Overhauser, A. W. Theory of the Dielectric Constants of Alkali Halide Crystals. *Phys. Rev.* **1958**, *112*, 90−103.
(53) Mott, N. F.; Littleton, M. J. Conduction in Polar Crystals. I. Electrolytic Conduction in Solid Salts. *Trans. Faraday Soc.* **1938**, *34*, 485−499.
(54) Gale, J. D.; Rohl, A. L. The General Utility Lattice Program (GULP). *Mol. Simul.* **2003**, *29*, 291−341.
(55) Saiful Islam, M.; Read, M. S. D.; D'Arco, S. From Oxides to Oxyhalides: Modelling the Properties of High TCsuperconductors. *Faraday Discuss.* **1997**, *106*, 367−376.
(56) Catlow, C. R. A Interionic Potentials for Alkali Halides. *J. Phys. C: Solid State Phys.* **1977**, *10*, 1395.
(57) Binks, D. J. Ph.D. Thesis, University of Surrey, Guildford, U.K., 1994.
(58) Islam, M. S. Defect Structure and Ion Transport in LaOBr. *J. Phys. Chem. Solids* **1990**, *51*, 367−372.
(59) Bush, T. S.; Gale, J. D.; Catlow, C. R. A.; Battle, P. D. Self-Consistent Interatomic Potentials for the Simulation of Binary and Ternary Oxides. *J. Mater. Chem.* **1994**, *4*, 831−837.
(60) Plimpton, S. Fast Parallel Algorithms for Short-Range Molecular Dynamics. *J. Comput. Phys.* **1995**, *117*, 1−19.
(61) Evans, D. J.; Holian, B. L. The Nose−Hoover Thermostat. *J. Chem. Phys.* **1985**, *83*, 4069−4074.
(62) He, X.; Zhu, Y.; Epstein, A.; Mo, Y. Statistical Variances of Diffusional Properties from Ab Initio Molecular Dynamics Simulations. *NPJ. Comput. Mater.* **2018**, *4*, 18.
(63) Wood, S. M.; Eames, C.; Kendrick, E.; Islam, M. S. Sodium Ion Diffusion and Voltage Trends in Phosphates $Na_4M_3(PO_4)_2P_2O_7$ (M = Fe, Mn, Co, Ni) for Possible High-Rate Cathodes. *J. Phys. Chem. C* **2015**, *119*, 15935−15941.
(64) Treacher, J. C.; Wood, S. M.; Islam, M. S.; Kendrick, E. Na_2CoSiO_4 as a Cathode Material for Sodium-Ion Batteries: Structure, Electrochemistry and Diffusion Pathways. *Phys. Chem. Chem. Phys.* **2016**, *18*, 32744−32752.
(65) Deng, Y.; Eames, C.; Chotard, J.-N.; Lalère, F.; Seznec, V.; Emge, S.; Pecher, O.; Grey, C. P.; Masquelier, C.; Islam, M. S. Structural and Mechanistic Insights into Fast Lithium-Ion Conduction in Li_4SiO_4−Li_3PO_4 Solid Electrolytes. *J. Am. Chem. Soc.* **2015**, *137*, 9136−9145.
(66) Deng, Y.; Eames, C.; Fleutot, B.; David, R.; Chotard, J.-N.; Suard, E.; Masquelier, C.; Islam, M. S. Enhancing the Lithium Ion Conductivity in Lithium Superionic Conductor (LISICON) Solid Electrolytes through a Mixed Polyanion Effect. *ACS Appl. Mater. Interfaces* **2017**, *9*, 7050−7058.
(67) Clark, J. M.; Nishimura, S. I.; Yamada, A.; Islam, M. S. High-Voltage Pyrophosphate Cathode: Insights into Local Structure and Lithium-Diffusion Pathways. *Angew. Chem., Int. Ed.* **2012**, *51*, 13149−13153.
(68) Dawson, J. A.; Tanaka, I. Oxygen Vacancy Formation and Reduction Properties of β-MnO_2 Grain Boundaries and the Potential for High Electrochemical Performance. *ACS Appl. Mater. Interfaces* **2014**, *6*, 17776−17784.
(69) Aparicio, P. A.; Dawson, J. A.; Islam, M. S.; de Leeuw, N. H. A Computational Study of $NaVOPO_4$ Polymorphs as Cathode Materials for Na-Ion Batteries: Diffusion, Electronic Properties and Cation Doping Behavior. *J. Phys. Chem.* DOI: 10.1021/acs.jpcc.8b07797.
(70) Reckeweg, O.; Blaschkowski, B.; Schleid, T. Li_5OCl_3 and Li_3OCl: Two Remarkably Different Lithium Oxide Chlorides. *Z. Anorg. Allg. Chem.* **2012**, *638*, 2081−2086.
(71) Hippler, K.; Sitta, S.; Vogt, P.; Sabrowsky, H. Structure of Na_3OCl. *Acta Crystallogr., Sect. C: Cryst. Struct. Commun.* **1990**, *46*, 736−738.

DOI: 10.1021/acs.jpcc.8b08208
J. Phys. Chem. C 2018, 122, 23978−23984